Arabian Journal of Chemistry (2022) **15**, 103862

King Saud University

Arabian Journal of Chemistry

www.ksu.edu.sa
www.sciencedirect.com

ORIGINAL ARTICLE

A facile approach to fabricate and embed multifunctional nano ZnO into soap matrix and liquid cleansing products for enhanced antibacterial and photostability for health and hygiene applications

Nitesh Bhalla [a,b,*], Nitin Ingle [b], Hiral Patel [b], Athira Jayaprakash [b], Srilakshmi V. Patri [a], Ajeet Kaushik [c], D. Haranath [d]

[a] *Department of Chemistry, National Institute of Technology, Warangal 506004, Telangana, India*
[b] *IFFCO Group, Seville Products LLC, Plot 24, Street 3B, Umm Ramool, PO Box 10596, Dubai, United Arab Emirates*
[c] *NanoBioTech Laboratory, Department of Environmental Engineering, Florida Polytechnic University, Lakeland, FL 33805, United States*
[d] *Department of Physics, National Institute of Technology, Warangal 506004, Telangana, India*

Received 13 January 2022; accepted 23 March 2022
Available online 28 March 2022

KEYWORDS

Surfactant-polyol-assembly (SPA);
Functionalized ZnO;
Health and hygiene applications;
Sodium salt of long chain fatty acids;
Antibacterial efficacy;
Photostability

Abstract This research demonstrates, a facile approach to fabricate the nano ZnO system in an unique combination of surfactant-polyol-assembly (SPA) acting as a caging agent restricting the ZnO crystallite size in nano-regime. This SPA is suitable for health and hygiene products and such optimized technique is among the very few researches exploring the impact of embedding low concentrations of nano ZnO system into the matrix of sodium salt of long chain fatty acids (soap bar) and liquid cleansing personal care products. The fabricated nano ZnO in SPA and infused products were systematically characterized using various advanced and appropriate techniques. The hexagonal wurtzite structure of nano ZnO-SPA is evaluated based on XRD pattern which also exhibit an average crystallite size as 20.18 nm and high specific surface area as 52.99 m^2/g. The SEM-supported morphological assessment confirms the formation of agglomerates of ultrafine ZnO rods and spherical particles. Novel nano ZnO having wideband gap energy (3.66 eV) embedded in soap bar act as a UV-blocker preventing the oxidation of unsaturated long chain fatty acids. Soap bar

* Corresponding author at: IFFCO Group, Seville Products LLC, Plot 24, Street 3B, Umm Ramool, PO Box 10596, Dubai, United Arab Emirates.
E-mail address: bhalla.nitesh@gmail.com (N. Bhalla).
Peer review under responsibility of King Saud University.

Production and hosting by Elsevier

https://doi.org/10.1016/j.arabjc.2022.103862

without ZnO experienced degradation and reduction in whiteness to 17.85% whereas 2.5 mg/g nano ZnO infused soap shows the reduction to 7.9% which clearly reflects the increased photostability of soap bar. The antibacterial efficacy of nano ZnO-SPA and infused products are investigated against *Staphylococcus aureus (S. aureus)* and *Escherichia coli (E. coli)* by Zone of Inhibition (ZOI) and European standard EN:1276. Infused products exhibited high antibacterial efficacy up to 4.43 log reduction equivalent to >99.99% germ kill.

1. Introduction

Nanoscale materials science have gained enormous attention in the last couple of decades, thereby transforming industries due to their advancements and influencing lives of people in various perspectives (Saleem et al., 2022; Nazir et al., 2021; Zhang et al., 2020; Rajamanickam and Shanthi, 2016; Imran et al., 2017; Samavati et al., 2021). Transition metal oxides have played an important role since ancient times and still plays an equally pivotal role in the era of nanotechnology with applications in diverse fields like medicine, polymer composites (Kumar et al., 2021), electronic technology (Mishra et al., 2021), solar energy (Khullar et al., 2016), personal care, cosmetic (Cole, 2016), food, photocatalytic activity (Isa et al., 2020; Rajapriya et al., 2019), bio sensing, light-emitting diodes, etc. ZnO nano systems have potential applications at room-temperature UV lasers (Huang, 2001), and transistor sensor (Cai et al., 2014), due to its exclusive optical & electrical properties like high chemical stability, low dielectric constant, having piezoelectric and photoelectric behaviors (Kong and Wang, 2003; Beasley and Meyer, 2010). ZnO is an important member of the wurtzite family having a hexagonal crystal lattice and wide bandgap II-VI group semiconductor. In this scientific work, authors aim to exploit the abundant properties of nanoscale ZnO to enhance the properties of health and hygiene products. Various routes to synthesize ZnO and their doped system have been reported in the literature comprising attrition method which involves the breaking of coarse particles into nano dimension using high energy ball mills (Wirunchit et al., 2021), solvothermal (Oprea et al., 2011), vaporization (Sánchez-Martín et al., 2021), combustion route (Vasile et al., 2012), sol–gel (Hasnidawani et al., 2016), assembly assisted (Goktas and Goktas, 2021) etc.

ZnO at nanoscale due to significant benefits such as tunable morphological characteristics, dimensional stability, and chemical stability, and have been adopted as a crucial material for several photonics and electronics based advanced applications (Haranath et al., 2004). As a result, investigation of structural factors becoming increasingly important for improving the efficiency of ZnO nanomaterial related applications. It has been suggested that not every metal oxide is allowed for cosmetic and personal care applications except a few like ZnO and TiO_2 (Smijs and Pavel, 2011). Among the five zinc compounds that are allowed as per the list of "General Recognized as Safe (GRAS)", ZnO is a one of the listed compounds which is approved by the Food and drug administration (FDA). Additionally, nanoscale ZnO has the following advantages (i) effective blocker against both UVA and UVB radiation unlike TiO_2 (ii) non-irritating (iii) well-suited with all types of skin (iv) shields against skin irritation and therefore highly used in personal care industry (Abendrot and Kalinowska-Lis, 2018). Although ZnO have been previously studied for antibacterial activities, this study aims to establish increased antibacterial efficacy of health and hygiene products using nano ZnO-SPA which remains barely studied in detail.

Key demerits associated with aforementioned synthesis methodologies are: (i) used solvents are expensive, possibly toxic and flammable (Goktas and Goktas, 2021) (ii) energy intensive techniques (Kumar et al., 2019) (iii) solvents or generated by-products are either not permitted or affects stability of health and hygiene products and (iv) introduce harmful marine ecosystems. Therefore, there is still a lot to unleash in ZnO fabrication methodologies as well as selection of appropriate precursors.

Additionally, major challenge nowadays is that conventional antibacterial agents used in sodium salt of long chain fatty acid (soap bars) and liquid cleansing products that have been in market for many decades are becoming extremely inefficient as antibacterial resistance grows throughout the world, making illnesses and death more problematic to manage. Most frequently used antibacterial agents such as Triclosan, Triclocarban, phenolic compounds and their carcinogenic by-products cause adverse effects, reproductive toxicity, highly destructive to the environment and are banned by the FDA since 2016 (Halden, 2014). Additionally, zinc pyrithione (ZPT) an antifungal agent with extensive use in anti-dandruff shampoos that has been banned in many countries as of 2022 despite years of commercial use (https://old.sfda.gov.sa/ar/cosmetic/SysImpReg/RESTRICTED_SUBSTANCES.pdf). Therefore, once common antibacterial agents are getting phased out from the personal care products in many countries. New antibacterial agents are hence desperately required for personal care products, keeping researchers on their toes as they explore new and effective actives to fight disease-causing microbes like *Staphylococcus aureus (S. aureus)*, *Escherichia coli (E. coli)* as well as recent world-wide pandemic Covid-19 causing respiratory syndrome. Furthermore, another major challenge is oxidation of unsaturated long chain fatty acids of soap bars causing photo-degradation under sunlight resulting into rancid and unpleasant yellow–brown colored product.

This research is aims to address the major concerns mentioned above in the health and hygiene products by fabricating multifunctional nano ZnO-SPA system. This work may be the first or among the very few reports where authors have explored this unique surfactant and polyol combination, perfectly suitable precursors for personal care industry that aid in keeping the crystallite size of ZnO in nano-regime. SLES is an anionic surfactant that is cost effective material that is commonly used in health and hygiene industry especially cleansing products. Glycerin is also a well-known co-surfactant for engineering nanoscale materials when additionally acts as humectant preventing the trans epidermal water loss to keep the skin moisturized (Lodén and Wessman, 2001). Therefore, presented SPA based nano ZnO synthesis strategy has several advantages such as high compatibility with health and hygiene, personal care products especially liquid cleansing products, non-toxic, low cost solvents, low energy consuming, non-intensive process and is a one-step fast synthesis without any additional process like calcinations and milling.

The current method takes advantage of unique properties of surfactant and polyol combination such as micellar formation and their cage-like matrix to synthesize ZnO in nanoscale and restricting the particle growth. This method thus uses assemblies and caging agents specifically to make synthesized ZnO suitable for industrial applications like health and hygiene, personal care and cosmetic products. The synthesized nano ZnO-SPA has high ZOI of 13 mm in comparison to recent development reports for titanium dioxide (TiO_2), zinc oxide (ZnO), and TiO_2/ZnO nanoparticles supported into 4A (alumina silicates) zeolite studied by Azizi et al. and hybrid films containing 1%, 2%, and 4% ZnO NPs studied by Santosh Kumar et al showing the ZOI of only 6–10 mm. (Azizi-Lalabadi et al., 2019; Kumar et al.,

2020). The synthesized nano ZnO-SPA possess high specific surface area 52.99 m^2/g compared to previously explored ZnO nanoparticles having only 25–27 m^2/g reported for ZnO nanoparticles synthesized by continuous precipitation approaches (Khezami et al., 2018; Boz et al., 2012).

Applications of fabricated nano ZnO-SPA for health and hygiene products by infusing it into sodium salt of long chain fatty acid (soap bars) and liquid cleansing products thereby significantly enhances the antibacterial efficacy established by conducting zone of inhibition and European standard EN 1276 against Gram-positive (*S. aureus*) and Gram-negative (*E. coli*) organisms. Embedding nano ZnO-SPA, a wide band gap inorganic UV blocker, in the soap bar reduces free radical generation thereby enhancing their photo-stability and minimize reduction of whiteness. This facile approach to fabricate multifunctional nano ZnO make it a potent and suitable material to use for various industrial applications.

2. Material and methods

2.1. Materials

Zinc chloride-97% [SD Fine-chem limited], distilled water pH of 5.5–7.0 with conductivity 1 μS/cm. Sodium Lauryl Ether Sulfate (SLES-2EO 70%), Cocamidopropyl Betaine (CAPB 30%) [Galaxy surfactant India], Glycerin (Polyol) [International Foodstuffs company (IFFCO) Malaysia, SDN BHD (IMSB)], Sodium hydroxide- 99% [VWR International], Soap noodles (65% Total Fatty Matter) [International Foodstuffs company (IFFCO) Egypt], Calcium nitrate, Methyl orange, Nitric acid, Phenol red indicator, Silver nitrate, Potassium chromate, Sulfuric acid, Ethylene glycol [SD Fine-chem limited]. Bacterial strains *Escherichia coli (E.coli)*ATCC 10,536 and *Staphylococcus. aureus (S.aureus)* ATCC 6538 were obtained from ATCC (American Type Culture Collection) in Dubai, UAE.

2.2. Synthesis of nano ZnO in SPA system

The SPA in aqueous medium prepared by taking 0.57 M SLES-2EO and 1.63 M of Glycerin. To the above mixture added 0.60 M of $ZnCl_2$ followed by stoichiometric steady addition of 1.23 M NaOH solution and with continuous stirring. The temperature maintained at 70–80 °C during reaction and mixed until uniform white homogeneous mix obtained indicating successful synthesis of nano ZnO-SPA. The reaction equation for synthesis of nano ZnO is as follows:

$$ZnCl_2 + 2NaOH \rightarrow Zn(OH)_2 + 2NaCl \quad (1)$$

$$Zn(OH)_2 \rightarrow ZnO + H_2O \quad (2)$$

Obtained morphologies in SEM correlates with proposed mechanism and hypothesis. Systematic and mechanistic presentation of synthesis of nano ZnO in SPA acting as caging agent is shown (Fig. 1A, B and C). The synthesized samples were centrifuged, washed, and dried for further evaluation.

2.3. Incorporation of nano ZnO-SPA in the matrix of sodium salt of long chain fatty acid

The synthesized nano ZnO-SPA were infused into the matrix of sodium salt of long chain fatty acid to establish the practical industrial applications. Sodium salt of long chain fatty acid matrix is incorporated with 0.5 mg/g, 1.5 mg/g, and 2.5 mg/g of nano ZnO-SPA. Mechanical process for soap manufacturing was followed such as mixing in sigma mixer, triple roll mill, and extrusion under vacuum to uniformly infuse nano ZnO-SPA into the sodium salt of long chain fatty acid.

2.4. Incorporation of nano ZnO-SPA in liquid cleansing product

Nano ZnO-SPA were incorporated into the liquid cleansing product having mixture of surfactant SLES-2EO, cocoamidopropyl betaine and other fundamental ingredients to establish the practical industrial applications. The liquid cleansing product was infused with different concentrations of nano ZnO-SPA i.e., 5 mg/mL, 10 mg/mL and 15 mg/mL and evaluated for antibacterial efficacy and other attributes.

2.5. Characterization methods of nano ZnO-SPA

UV–Visible spectrums were recorded by using UV–Vis spectrophotometer Model-1800 from Shimadzu, Japan in the absorbance range of 200–700 nm. The diluted suspension of nano ZnO-SPA was prepared in demineralized water and subjected to sonication for 5 min before recording the UV–Vis spectrum. FTIR spectrums were recorded by using Model-IRAffinity-1S make by Shimadzu, Japan. attenuated total reflection (ATR) from SPECAC, U.K. measurement mode was transmittance vs wavenumber, Scanning-45, spectrum recorded through ATR. The surface morphology of powdered nano ZnO-SPA was investigated by using SEM Model-JSM-6010 PLUS ILA in the range magnification of 2000x to 6000x, parameter was 20 kV, WD 12 mm, SS50. The elemental analysis of powdered nano ZnO-SPA was estimated by Energy Dispersive X-ray spectroscopy (EDS). The qualitative and quantitative analyses of nano ZnO-SPA system were done by using EDX-8100-Shimadzu, Japan. Nano ZnO-SPA was placed in sample holder and measurement was done using 10 mm collimator. The crystalline structure, size and phase analysis of nano ZnO-SPA was determined by using X-ray diffractometer (XRD Shimadzu-6100) having parameters CuK1 radiation (λ = 1.54056 Å), Voltage 40 kV, Current 30 mA, and scanning range 20°-70° 2θ. The rheological properties of the SPA, nano ZnO SPA and other materials were studied at 25 °C using Brookfield Rheometer DV3T model, using spindle RV-2 and RV-5 at RPM-12. The pH values were measured at 25 °C using pH meter Mettler Toledo model SevenCompact S220.

2.6. Characterization methods of sodium salt of long chain fatty acid matrix

The crystalline phase and size of sodium salt of long chain fatty acid matrix was analyzed by XRD. The surface morphology and qualitative and quantitative elemental analysis sodium salt of long chain fatty acid matrix infused with nano ZnO-SPA was analyzed by SEM. The XRD and SEM parameters mentioned in Section 2.5.

The estimation of long chain fatty acids composition in soap matrix was performed using GC Agilent Technologies-7820A having capillary column HP 5MS (30 m × 0.25 mm

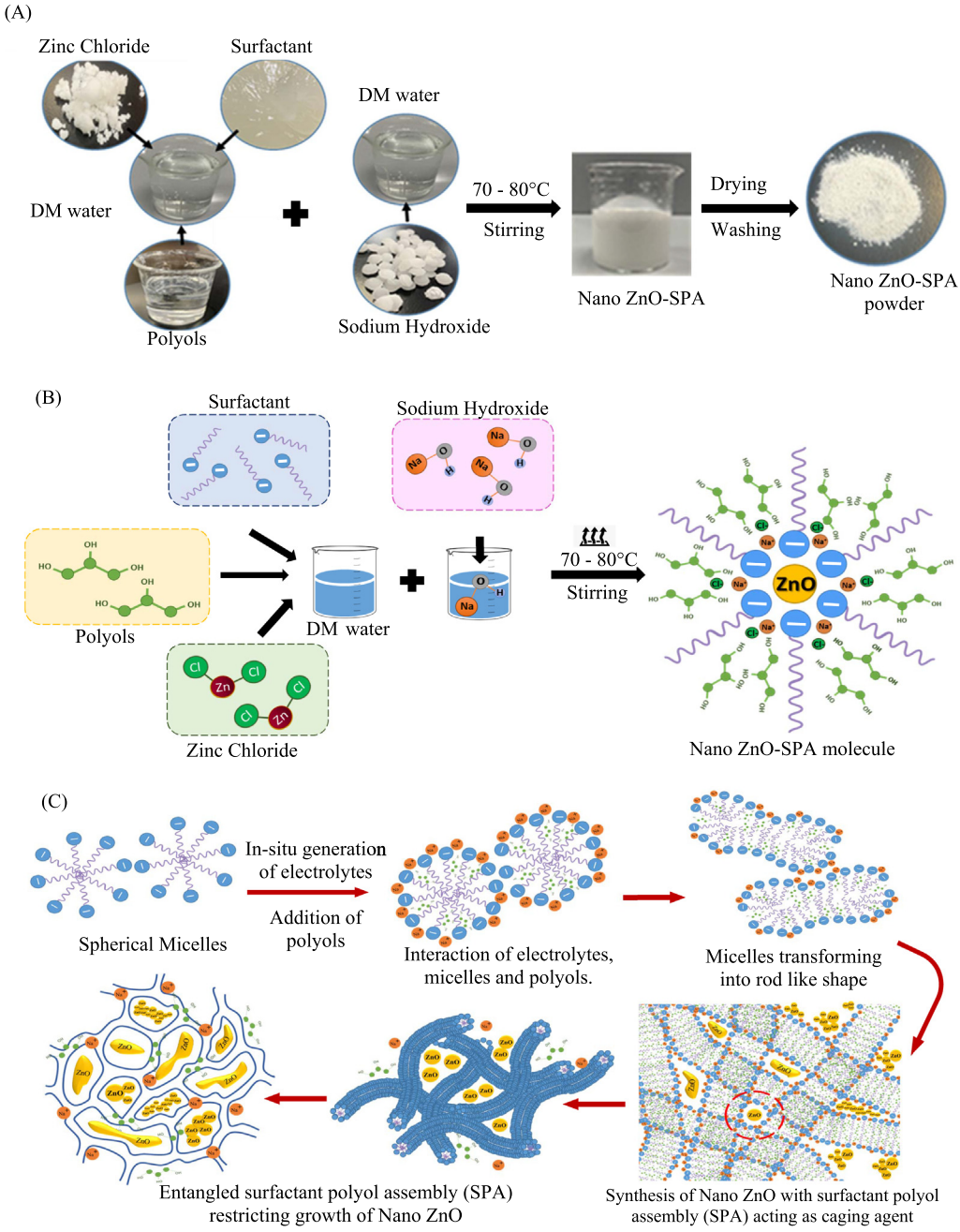

Fig. 1 (A and B) Systematic and mechanistic presentation to fabricate nano ZnO in SPA (C) Illustrative mechanism of caging of nano ZnO in SPA.

ID × 0.25 µm) in conjunction with 5% diphenyl 95% dimethylpolysiloxane. Electron ionization energy 70 eV, helium gas (99.99%) used as carrier gas with a constant flow rate 1 mL/min. The injection volume is 1 µL with a split ratio of 50:1, temperature 60 °C and ion source temperature 250 °C.

Chloride content was estimated using the following method: Dissolved 5 g of test sample in distilled water and added calcium nitrate solution. The resultant solution was filtered through Whatman filter paper, followed by addition of methyl orange as an indicator and dilute nitric acid to neutralize the solution. This solution was further subjected to titration with silver nitrate solution, using potassium chromate solution as endpoint indicator. Carry out a blank determination using the same quantity of all reagents but except the sample (IS 13498, 1997).

Further, the foamability was also analyzed using the following method. The aqueous solution of known quantity of soap bar was prepared and poured into a blender jar and blended at low speed for exactly 30 sec. Poured the generated foam quickly into the cylinder and measured the foam volume immediately after levelling off the top surface of the foam and noted the top height only.

2.7. Characterization methods of liquid cleansing products

The chloride content of liquid cleansing product was estimated by using method mention in Section 2.6. The rheological properties of liquid cleansing product having different concentration of nano ZnO-SPA (5 mg/mL, 10 mg/mL and 15 mg/mL) were studied on Brookfield Rheometer DV3T model, using spindle RV-5 for ZnO-SPA, RV-2 for rest of solutions at RPM-12, temperature-25 °C, torque more than 10, test duration 1 min. Initial calibration of Rheometer was done using standard having known viscosity in centipoise (cps).

2.8. Antibacterial properties and application of nano ZnO-SPA, soap matrix and liquid cleansing product

The antibacterial properties of nano ZnO-SPA, soap matrix and liquid cleansing product were evaluated by using disk diffusion method and European Standard log reduction method EN 1276:2019. Photostability test was conducted on sodium salt of long chain fatty acid (Soap matrix) to study the application and role of nano ZnO-SPA under direct sunlight.

2.8.1. Disk diffusion technique (ZOI)

Disk diffusion technique was used for evaluating the antibacterial efficacy of nano ZnO-SPA, SPA, AR grade ZnO and liquid cleansing product against both Gram-positive and Gram-negative bacteria i.e., *S. aureus* and *E. coli* respectively. These bacteria were selected as these are well known to cause various diseases among human being and animals. The bacterial strain was grown overnight and through UV spectrophotometer the optical density was adjusted to 0.1 at 600 nm to achieve 10^8 cfu/mL. The bacterial strains were spread homogeneously onto Muller & Hilton agar plates and allowed to dry. Sterile 6 mm disk were soaked in different concentration of test samples for 30 min and placed over the surface of Muller & Hilton agar plates. These plates were incubated at 37 °C for 24 h, and the inhibitory actions in diameter (mm) were revealed by a clear zone. (Azizi-Lalabadi et al., 2019; Kumar et al., 2020; Jin and Jin, 2021).

2.8.2. EN 1276:2019

Quantitative suspension test was used for the assessment of bactericidal activity of sodium salt of long chain fatty acid using EN 1276:2019 standard log reduction method. 1:1 diluted test sample was utilized and exposed with test organism suspension for contact time of 1 min followed by neutralization for specific time. Placed 1 mL of above mix on agar plate and incubated for 48 h at 37 °C.

2.8.3. Photostability study

The sodium salt of long chain fatty acid infused with and without nano ZnO-SPA were placed under direct sunlight for 10 days. Their photostability studies were performed by measuring their change in L, a, b values (color) using Xrite Ci 4200 (reflectance spectrophotometer) to evaluate and establish protecting effect of nano ZnO-SPA in the soap bar matrix under direct sunlight comprising high energy UV-rays. The spectrophotometer was calibrated by using white standard and black light trap standard and color ordinate measurement (L, a, b value) of test sample was measured every 2 days.

3. Results and discussions

3.1. Characterization of nano ZnO-SPA

3.1.1. UV–Visible spectroscopic studies

Optical absorption spectra of synthesized nano ZnO-SPA and AR grade ZnO was recorded in the range of 200–700 nm. The absorption spectroscopy shows the typical peak absorption of ZnO in UV region and the band gap energy was determined by plotting Tauc plot. The analytical grade ZnO exhibits the absorption peak at 386 nm with energy band gap (E_g = 3.21 eV) correspondingly nano ZnO-SPA exhibit the blue shift with absorption peak at 338 nm reflecting higher energy band gap (E_g = 3.66 eV) (Fig. 2A, B and C). Blue shift of UV spectra is observed with particle size reduction of nano ZnO-SPA with respect to bulk AR grade ZnO. This could be due to multiple reasons however, can attributed to quantum confinement effect which describes that band gap energy is inversely related to particle size, and shows a blue shift as the particle size decreases (Debanath and Karmakar, 2013). When the size of the particle decreases and approaches the size of the electron-hole distance, the energy levels of that particle becomes quantum confined and discrete thus confining the motion of electron (Goktas et al., 2018). Other possible reason of blue shift could be Burstein-Moss effect which is normally more prevalent in doped system and nanowires (Yang et al., 2007). It is also apparent that significant sharp absorption of nano ZnO synthesized in SPA reflects the narrow size distribution of the nano ZnO.

3.1.2. Fourier-transform infrared spectroscopy (FTIR) for functionality assessment

FTIR spectrum of Surfactant (SLES), Polyol (Glycerin), Surfactant polyol assembly- SPA, nano ZnO-SPA and AR grade ZnO exhibits the functional group in the following different regions (Fig. 3(A, B, C, D and E)), fingerprint region (<1500 cm^{-1}), double bond region (1500–2000 cm^{-1}), triple bond region (2000–2500 cm^{-1}), single bond region- 2500–4000 cm^{-1}). Spectrum (A, B, C and D) exhibits the sharp broad peaks in the range of 3361 cm^{-1}–3458 cm^{-1} in single bond region it evidently specifies the existence of hydroxyl (OH) group which can be attributed to the presence of polyol (glycerol) used during synthesis and H_2O molecules. Two weak peaks at 2924 cm^{-1} & 2852 cm^{-1} observed in spectrum (A, B, C and D) are due to C-H stretching: one for symmetrical and other for asymmetrical vibrational frequency. This evidently stipulate the existence of a long-chain linear aliphatic compound of SLES-2EO surfactant. While peaks at 2351 cm^{-1} and 2368 cm^{-1} in spectrum (C and D) can be attributed to O═C═O stretching possibly due existence of impurity during synthesis or measuring environmental conditions. The peak at 1637 cm^{-1} in spectrum (A, C and D) could be related moisture or to the impurity coming through the SLES used during the synthesis. The two peaks at 1465 cm^{-1} and 781 cm^{-1} in spectrum (A) could be because of long chain linear aliphatic compounds. The peak at 1215.15 cm^{-1} exhibit the existence of S═O vibrations of sulfur-oxy compounds in SLES-2EO (Peretz et al., n.d.; Cunliffe et al., 2020). The peak at 1110.9 cm^{-1} in spectrum (B, C and D) is due to the C-O stretching vibration of secondary alcohol group while peak

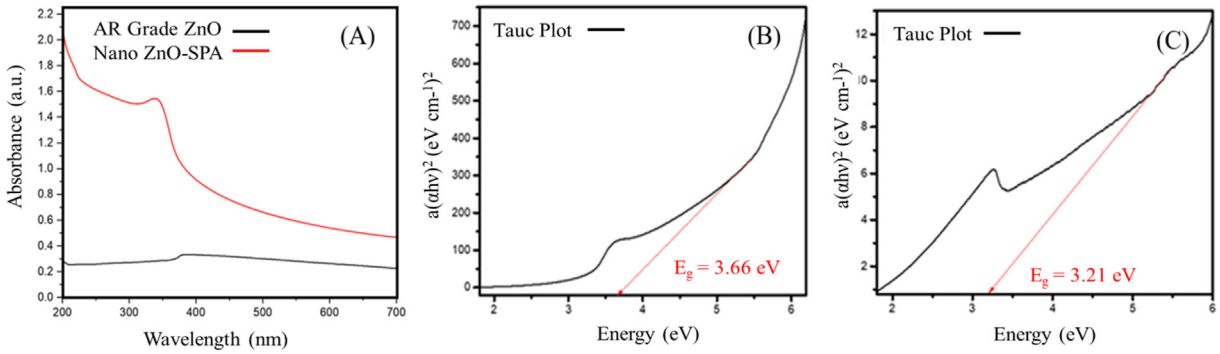

Fig. 2 (A) UV–Vis spectra of nano ZnO synthesized in SPA and spectrum of AR Grade ZnO. Tauc plots of $a(\alpha h\nu)^2$ (eV $cm^{-1})^2$ as function of photon energy hν (eV) for (B) nano ZnO and (C) AR Grade ZnO.

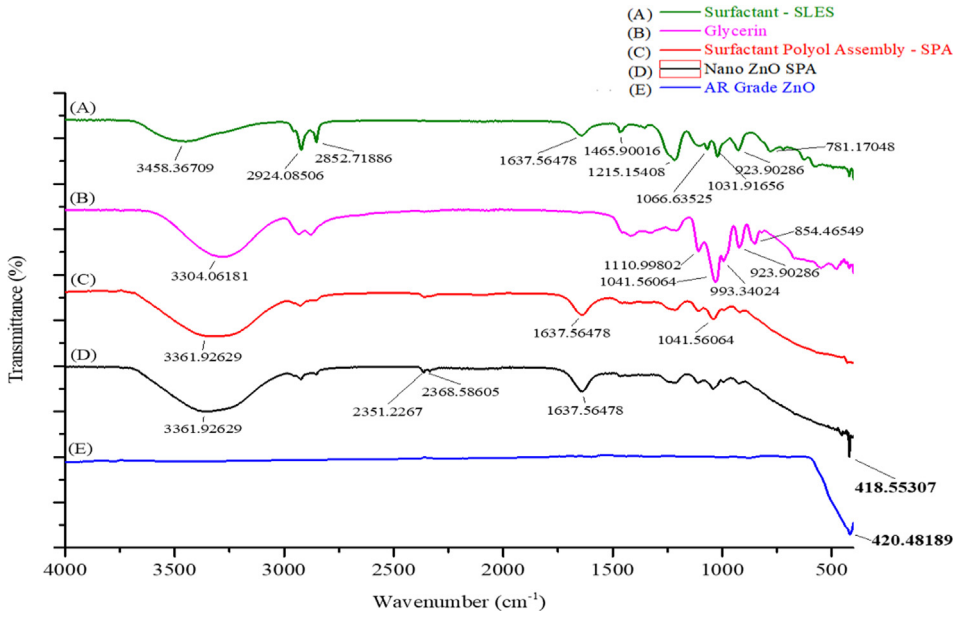

Fig. 3 FTIR spectrum of (A) Surfactant- SLES (B) Glycerin (C) Surfactant polyol assembly- SPA (D) Nano ZnO-SPA and (E) AR Grade ZnO in the spectral range of 400–4000 cm^{-1}.

around at 1041 cm^{-1} and 1031 cm^{-1} in spectrum (A, B, C and D) suggest deformation vibration of (CH) + (C—C) (Hammoudeh et al., 2020). The peak at 993 cm^{-1} in spectrum (B, C and D) indicate the existence (C—C) vibration. The peak at 923 cm^{-1} and 854 cm^{-1} in spectrum (A, B, C and D) could be attributed for asymmetric C—O—C stretching of surfactant and polyol molecules. The peak in spectrum (D) at 418.55 cm^{-1} shows the presence of nano ZnO similar to AR grade ZnO peak at 420 cm^{-1} shown in spectrum (E). Several literatures stated the ZnO peak at 410 cm^{-1} to 440 cm^{-1}. These results are in line with reported research work (Hasan et al., 2021).

3.1.3. X-Ray diffractometer (XRD) analysis for purity assessment

The crystalline structure of nano ZnO-SPA and AR grade is shown in (Fig. 4A and B). XRD peaks of powder nano ZnO synthesized in SPA confirms the hexagonal wurtzite structure and the results agree with the results reported by other literatures (Lei et al., 2012). The diffraction peaks of nano ZnO-SPA is distinguished at 2θ of 32.05°, 34.69°, 36.52°, 47.78°, 56.82°, 63.06°, 66.58°, 68.14° and 69.26° (Table 1). The observed planes for both the samples are well aligned with JCPDS 36–1451, Fig. 4(C). Sharp and intense peaks reflect the high crystallinity of the synthesized ZnO. The average crystallites size of nano ZnO-SPA is 20.18 nm (Table 1) and AR grade ZnO is 30.87 nm (Table 2) enumerated using the Debye-Scherrer equation,

$$D = K\lambda/\beta\ cos\theta \qquad 3)$$

D-crystallites size, λ-The wavelength of X-ray, K-Scherrer constant (0.9), θ-Braggs angle in radians, β-Full width at half maxima of the peak in radians.

Specific surface area evaluation: Specific surface area is property of solid materials which measure total surface area per unit mass of bulk volume, solid or cross-sectional area. The specific surface area can be evaluated by using following equation,

$$S = 6 \times 10^3/D_P \times \rho \qquad (4)$$

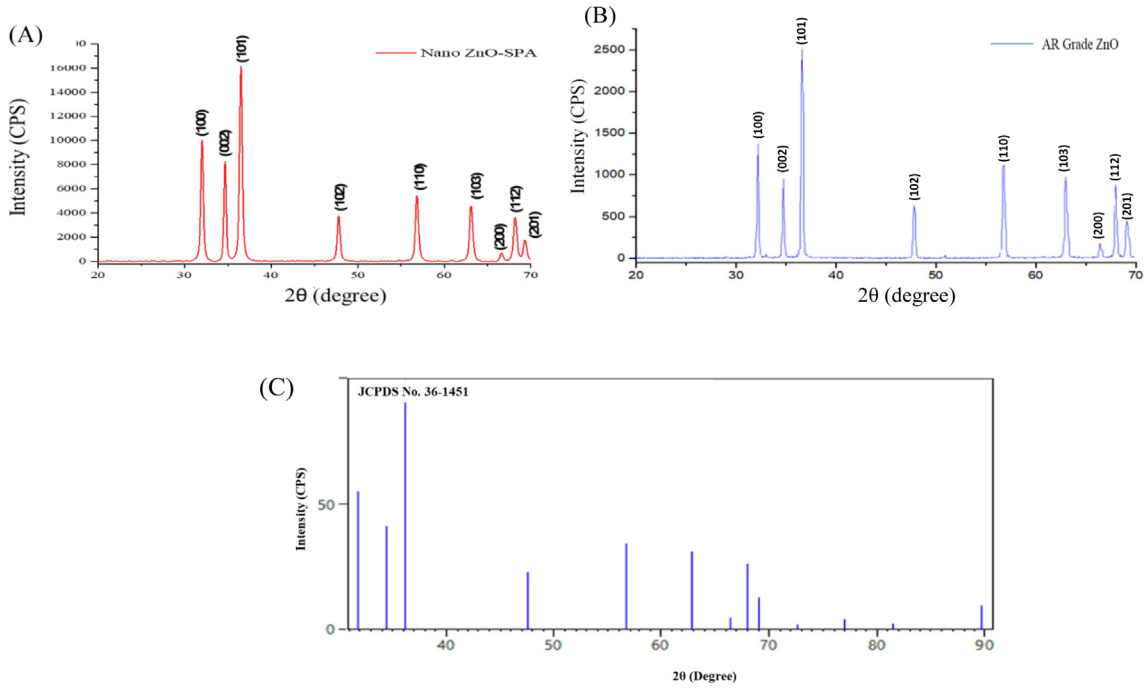

Fig. 4 (A) XRD pattern of nano ZnO-SPA, (B) XRD pattern of AR Grade ZnO (C) JCPDS ZnO standard card for reference.

Table 1 Crystallites size and miller index of nano ZnO-SPA by XRD.

Sr. No.	Peak Position 2θ (Degree)	d-spacing (Å)	FWHM (deg)	Crystallite size D (nm)	Average crystallite size D (nm)	Miller Indices
1	32.0506	2.7903	0.3381	22.583	20.18	(100)
2	34.687	2.5832	0.2944	25.757		(002)
3	36.52	2.458	0.3594	20.991		(101)
4	47.78	1.9019	0.3471	20.926		(102)
5	56.82	1.619	0.3481	20.073		(110)
6	63.06	1.4729	0.3559	19.026		(103)
7	66.58	1.4034	0.3567	18.616		(200)
8	68.14	1.375	0.3757	17.515		(112)
9	69.26	1.3553	0.4032	16.212		(201)

Table 2 Average crystallite size, lattice parameter and bond length of nano ZnO-SPA and AR grade ZnO using XRD.

Nanomaterial	Average crystallite size (nm)	Lattice parameters (Å)		Average dislocation density (δ) (lines/m^2)	u	c/a ration	Bond Length (Å)	Specific surface area (m^2/g)
		a	C				L	
Nano ZnO-SPA	20.18	3.22	5.16	0.002	0.44	1.6034	1.882	52.99
AR Grade ZnO	30.87	3.27	5.24	0.0017	0.44	1.6008	1.911	41.34

where S- Specific surface area, D_P – size of particle, ρ- density of ZnO 5.61 g/cm^3.

The specific surface area of nano ZnO-SPA crystallites was found to be 52.99 m^2/g which is relatively higher specific surface area than AR grade ZnO which is 41.34 m^2. g^{-1} as seen in Table 2. High specific surface area could be due to obvious reason of miniaturization of particle size which is inversely proportional to specific surface area. This high specific area can play a vital role to contribute towards the high antibacterial efficacy of nano ZnO-SPA due to high surface availability and disrupting the cell wall of disease-causing germs.

Lattice Parameter evaluation: The lattice parameters a, b and c of nano ZnO-SPA and AR grade ZnO structures were calculated by using the following equations:

$$\frac{1}{d_{hkl}^2} = \frac{4}{3}\left(\frac{h^2 + hk + k^2}{a^2}\right) + \frac{l^2}{c^2} \quad (5)$$

where for hexagonal unit cell lattice $a = b \neq c$, λ -wavelength of the XRD, n- order of diffraction, d_{hkl}- interplanar spacing, hkl is the Miller indices. The XRD analysis reveal peaks consistent to hexagonal wurtzite ZnO crystals with (hkl) values corresponding to that of standard JCPDS card Table.1. The lattice parameter of nano ZnO-SPA is found to be a = 3.22 and c = 5.16 while the c/a ratio is 1.6034. The lattice parameter of AR grade ZnO is found to be a = 3.27 and c = 5.24 while the c/a ratio is 1.6008 which is tabulated in Table 2.

The length of dislocation lines per unit volume (dislocation density) of nano ZnO-SPA and AR grade ZnO is 0.002 and 0.0017 lines/m^2 respectively calculated using the equation:

$$\delta = \frac{1}{D^2} \quad (6)$$

Dislocation density is the measure of defects in a system, when there is a rise in density of delocalized electrons due to high defects the attraction of delocalized electrons and nuclei increases thus increasing stability. Rise in density of delocalized electrons have also been known to provide energetic surface to nanoparticles due to increase in percentage of surface atoms (Gnanamozhi et al., 2020; Shaban et al., 2018; Gomathi et al., 2018). This factor contributes highly in the antibacterial efficacy of nano ZnO-SPA.

The Zn—O bond length of nano ZnO-SPA and AR grade ZnO is 1.882 and 1.911 Å respectively calculated by the following equation.

$$L = \sqrt{\frac{a^2}{3} + \left(\frac{1}{2} - u\right)^2 c^2} \quad (7)$$

where, u parameter in the wurtzite structure of nano ZnO-SPA and AR grade ZnO is 0.44 calculated by following equation.

$$u = \frac{a^2}{2c^2} + 0.25 \quad (8)$$

3.1.4. Scanning electron microscope analysis

The surface morphology analysis of powdered nano ZnO-SPA was done by scanning electron microscopy (SEM, JSM-6010 PLUS ILA) Fig. 5(A, B and C). Nano ZnO-SPA appeared as ultrafine rods and white spherical dots in the images with a size around 500 nm as associated with the scale. The ZnO nanoparticles asymmetrically distributed on the surface shows the agglomeration. These morphologies of nano ZnO could be due to their growth in restricted entangled cage of rod like micelles of surfactant formed in the presence of polyol and electrolyte (NaCl) generated as by product during the reaction. This electrolyte contributes towards the reduction of the gap between negative head group of surfactants resulting in the change of surfactant packing parameters and shifting the shape of micelles more towards rod like from spherical shapes. These rod-like micelles entangled with each other and enhance the viscosity of medium to a certain extent and act as caging matrix to restrict the particle growth. The EDS exhibits the quantitative elemental composition of nano ZnO powder at different sites (Fig. 5 (A, B and C)) which reflect the high purity with the elemental composition of mass % Zn – 79.64 and O – 20.36, Zn – 88.97 and O – 11.03, Zn – 77.50 and O – 22.50 shown in Fig. 5(D, E and F).

3.1.5. EDX-assisted elemental evaluation of nano ZnO-SPA systems

The EDX is the utmost imperative technique for quantitative elemental analysis. Nano ZnO-SPA shows the expected stoichiometric mass of 53.33% ZnO, 28.30% Cl ions, generated as a byproduct in the reaction and 18.07% sulfur trioxide (SO_3) which could be from presence of surfactant (sodium lauryl ether sulfate-2EO) in the sample (Table 3) while SO_3 is not present once powdered as seen in above section (Fig. 5 D, E and F). Strong peaks exhibit of ZnKα evidently confirms the presence of ZnO which is synthesized in SPA (Bahadur et al., 2007).

The strong peaks of ZnO measured from the line ZnKα and the 3-sigma value is 0.113 with an intensity of 3362 (cps/uA). Chloride (Cl) peak exhibits from line ClKα and the 3-sigma value 0.47, intensity 50.8533 (cps/uA), sulfur trioxide (SO_3) measured from line SKα, 3-sigma value- 0.25, intensity 5.547 (cps/uA).

3.1.6. Rheological properties and pH of nano ZnO-SPA

The rheological property (viscosity) of the synthesized nano ZnO-SPA, SPA and other materials were evaluated using Brookfield Rheometer and found to be 2300 cps and 6.07 cps for nano ZnO-SPA and SPA respectively (Table 4). The in-situ generation of sodium chloride electrolytes during fabrication of nano ZnO-SPA in surfactant (SLES-2EO) and polyol medium cause the conversion of hexagonal surfactant micelles to rod shape micelles, this leads to increased viscosity compared to SPA. The pH of nano ZnO-SPA was found to be 7.60 which is in neutral range thus causing minimal to no effect in the pH of final products. The pH of SPA and all materials used for synthesis of nano ZnO-SPA have been tabulated in Table 4.

3.2. Evaluation of sodium salt of long chain fatty acid

Different concentration of nano ZnO-SPA added into the soap matrix and their characterization was performed using XRD, SEM, and physiochemical analysis.

3.2.1. XRD analysis of soap matrix

This could be the first or among the very few published scientific reports on XRD studies of sodium soap infused with nano ZnO synthesized in surfactant polyol assembly. Cation-specific interactions with carboxylate of long chain fatty acid have strong ionic forces that govern the crystalline phases of fabricated soaps. Additionally, weak van der Waals interactions between the C-H bonds in the fatty acids chain also plays a major role in soap's crystalline phases (Jandacek and Broering, 1989). XRD patterns can be used to identify the crystalline phases of fabricated soap. It has been previously stated that sodium soap occurs in four crystalline phases namely, alpha, beta, delta, and omega. Intensity vs diffraction angles are plotted on Fig. 6 to better observe the degree of crystallinity and pattern sharpness. However, it must be noted that relative intensity depends on crystal type as well as the

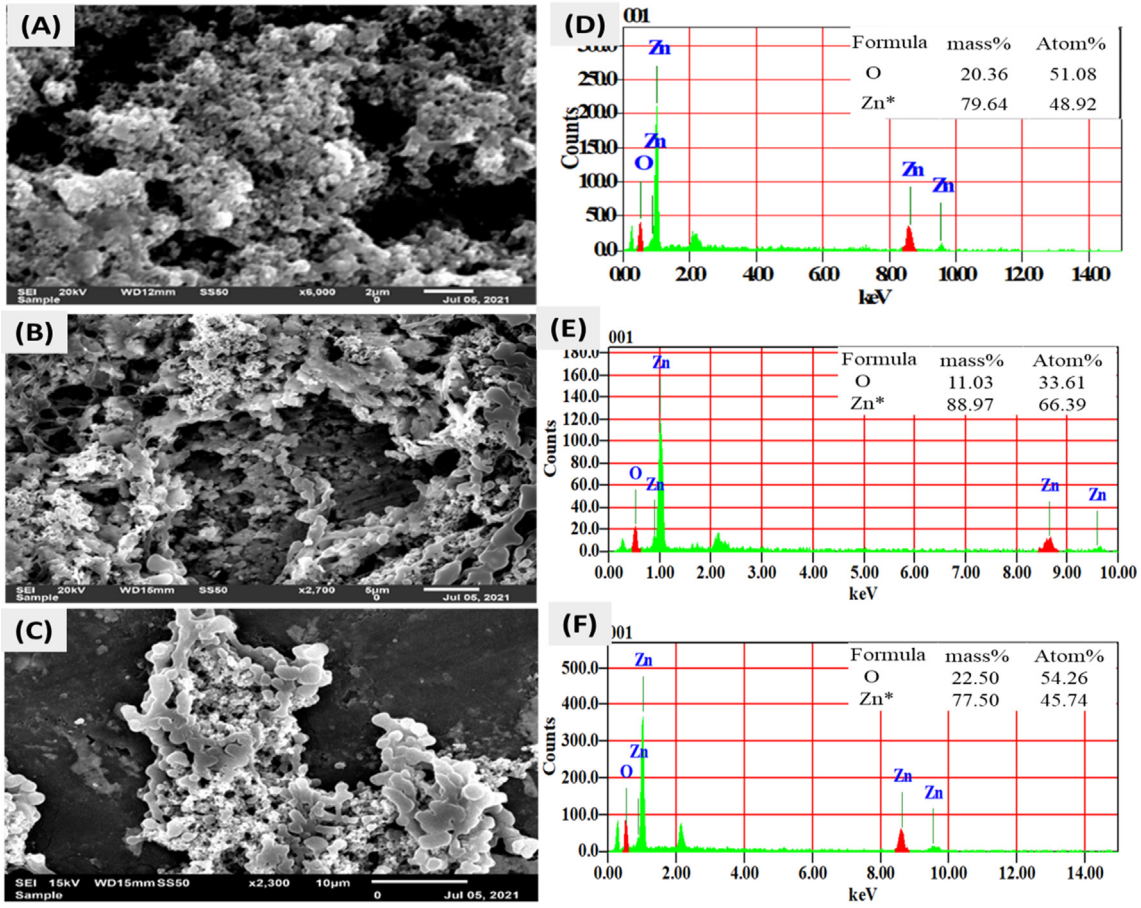

Fig. 5 (A, B and C) Representative SEM images of powdered nano ZnO-SPA, (D, E and F) EDS of powdered nano ZnO-SPA revealing the elemental composition in graphical and tabulated form respectively.

Table 3 Quantitative elemental analysis of nano ZnO-SPA by EDX.

Analytes	Result %	[3-sigma]	Line	Int.(cps/uA)
ZnO	53.33	0.11	ZnKα	3362.33
Cl	28.33	0.47	ClKα	50.85
SO_3	18.08	0.25	SKα	5.54

scattering power of X ray atoms and thus may show discrepancy from soap to soap (Hattiangdi, 1949). XRD results reveal peak position, d spacing and intensity results in Table 5. The peaks observed at 10.77, 39.97 and 42.61 can be attributed to delta, omega, and beta phases of sodium palmitate respectively while the peaks at 51.85 is characteristic of alpha phase sodium stearate. Furthermore, peak at 30.46 having d spacing of 2.93 Å can be representative of sodium oleate. The peak at 32.79 having d spacing of 2.72 Å can be attributed to nano ZnO. The average crystallite size of soap was 7.51 nm.

Table 4 pH and viscosity of nano ZnO-SPA and constituents.

Sr. No.	Name of material	pH value	Viscosity (cps)
1.0	Surfactant Polyol Assembly (SPA)	7.30	6.07
2.0	Nano ZnO-SPA	7.60	2300
3.0	Zinc Chloride (0.61 M solution)	5.02	2.05
4.0	NaOH (1.23 M solution)	14.0	3.09
5.0	Surfactant (SLES 2EO) (0.57 M solution)	7.40	5.80
6.0	Polyol (Glycerin) (1.63 M solution)	5.50	4.01

3.2.2. SEM analysis of soap matrix

The SEM is an imperial tool to examine the surface morphology. The morphological evaluation of sodium salt of long chain fatty acid infused with nano ZnO-SPA done by using SEM. Different surface morphology images of soap matrix was examined revealing their layered and intercon-

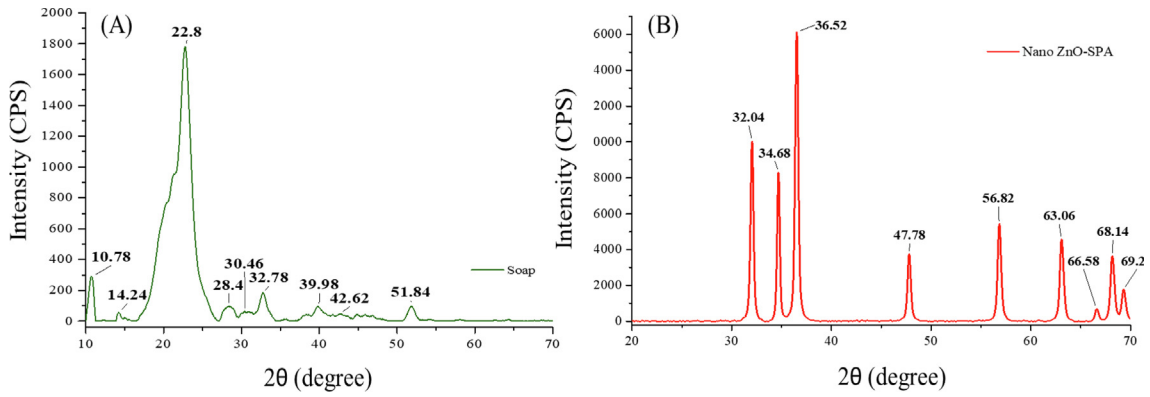

Fig. 6 (A) XRD pattern of sodium salt of long chain fatty acid infused with nano ZnO-SPA (B) XRD pattern of nano ZnO-SPA.

Table 5 Crystallite size of sodium salt of long chain fatty acid infused with nano ZnO-SPA by XRD.

Sr. No.	Peak Position 2 Theta (deg)	d-spacing(Å)	Intensity(I/I1)	FWHM(deg)	Crystallite sizeD (nm)	Average crystallite size D (nm)
1	10.7768	8.20282	197	0.75100	10.5313	7.5177759
2	14.3236	6.17863	40	0.53330	14.7799	
3	18.1479	4.88431	99	1.17340	6.68542	
4	20.4216	4.34534	520	2.86000	2.73366	
5	22.7956	3.89789	1199	1.80540	4.3134	
6	25.9693	3.42828	59	0.71000	10.9028	
7	28.4005	3.14009	69	1.71000	4.50371	
8	30.4627	2.93205	46	1.34660	5.69214	
9	32.7967	2.72852	126	1.08670	7.01291	
10	39.9739	2.25362	65	1.44000	5.18445	
11	42.6121	2.12000	36	2.50000	2.96045	
12	51.8540	1.76179	68	1.06670	6.69778	

nected structure. Additionally, distribution of spherical ZnO nanoparticles and certain voids observed which also seem to be occupied by nano ZnO confirmed with further focusing on these particles and conducting the EDX (Fig. 7A-F). These layered structure and disruptions could be due to high shear experienced by soap during the processing like sigma mixer, roll mills and extrusion which may alter the inherent structure and rearrange the matrix. Table 6 shows the elemental analysis of soap matrix infused with nano ZnO exhibits the presence of 68.48% carbon (C) due to soap have long carbon chain fatty acids, 15.7% oxygen (O) molecule can be due to nano ZnO-SPA and $-COO^{-}$ Na^{+} group of soap, 13.17% sodium (Na) exhibits sodium salt of soap, 1.37% chloride (Cl) and 1.27% of zinc (Zn) molecule which is infused in soap.

3.2.3. Estimation of fatty acid composition by GC-FID

The fatty acid composition estimation of soap bar was performed using flame ionization detector (FID). Lauric, myristic, palmitic, stearic, oleic and linoleic acids are at 5.45%, 1.51%, 50.12%, 5.2%, 29.5%, and 6.9% which described in the Table 7**.** These estimated fatty acid percentages indicate a 90:10 oil blend soap having 90% palm oil (PO) and 10% palm kernel oil (PKO). Where PKO contains approximately 50% lauric acid while palmitic acid and oleic acids are abundantly present in PO.

3.2.4. Estimation of chloride content

Different concentrations of nano ZnO-SPA were added into the soap matrix, the chloride content into the soap matrix significantly changes from 0.5% to 0.85% which is within acceptable limits (Table 8)**.** The electrolyte plays an important role in molecular arrangement and formation of the soap phases. The electrolyte will salt-out the soaps due to ionic strength and common ion effect in the liquid phase. The result will be reducing the volume of the liquid phase and increasing the solid phase and hardness of soap (Hall, 2016). Increase in the electrolyte (NaCl) in soap from 0.5 to 0.85% increases the hardness significantly and beyond 1% can have detrimental effects on soap cracking attribute.

3.2.5. Foamability test

The impact on foamability due to addition of different concentrations of nano ZnO-SPA into soap matrix was studied and recorded the significant difference in the foam of soap infused with nano ZnO-SPA as compared to the base formulation.

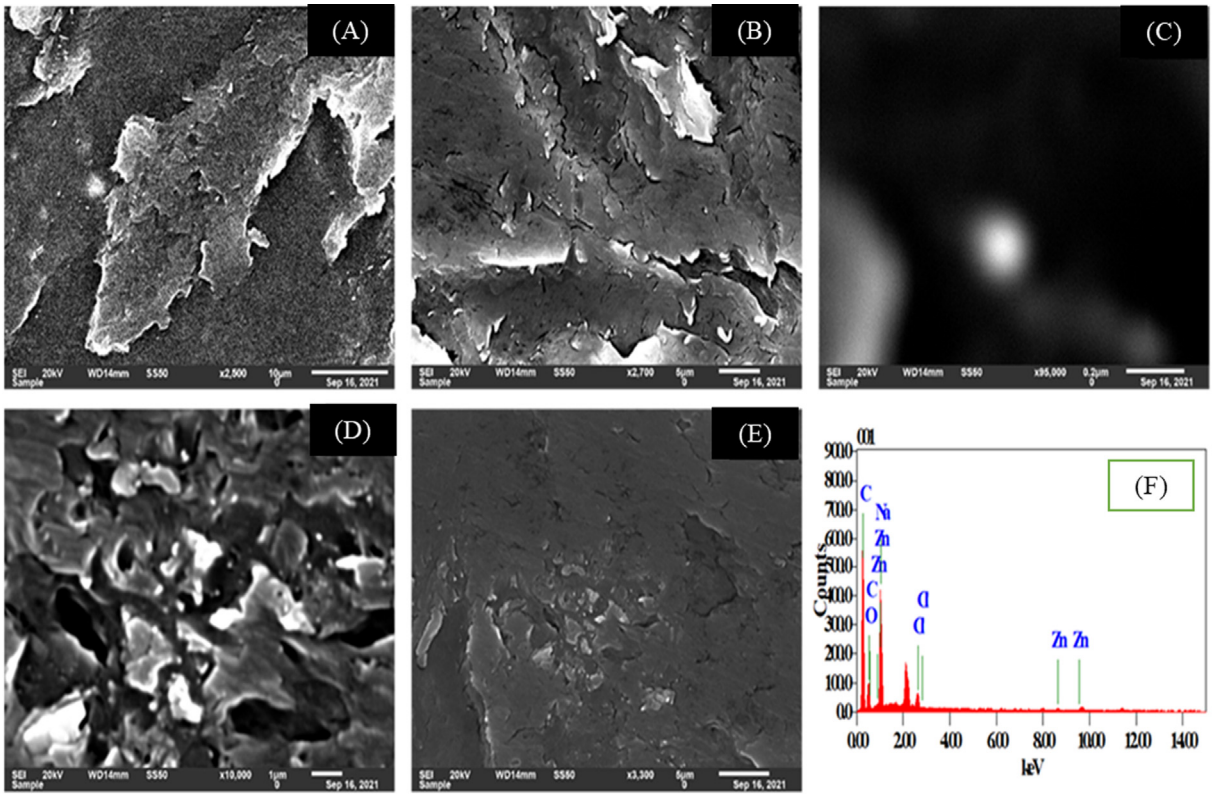

Fig. 7 (A-E) SEM imaging and (F) EDAX-based elemental assessment of soap matrix infused with ZnO-SPA nano system.

Soap infused with ZnO-SPA nano system exhibited up to 28% increase in the foam in comparison to base formulation (Table 8). This could be due to extra surfactant coming into soap matrix along with nano ZnO-SPA. This additional surfactant plays role in influencing the critical micelle concentration (CMC) of soap and enhancing the foamability.

3.3. Evaluation of liquid cleansing product infused with nano ZnO-SPA

Varying concentrations of nano ZnO-SPA were added into the liquid cleansing product and studied the effect of nano ZnO-SPA on various attributes of liquid product.

Table 6 Quantitative elemental analysis of sodium salt of long chain fatty acid infused with nano-ZnO-SPA by EDX.

Formula	Mass%	Atom%	Sigma	Net	K ratio Line
C	68.48	77.95	0.13	12,162	0.0059 K
O	15.70	13.42	0.26	2181	0.0036 K
Na	13.17	7.83	0.16	12,148	0.0108 K
Cl	1.37	0.53	0.05	2029	0.0016 K
Zn*	1.27	0.27	0.20	309	0.0012 K
Total	100				

Table 7 Fatty acid composition of sodium salt of long chain fatty acid by GC-FID.

Sr. no	Name of Fatty acid	Molecular formula	Chain length	% by GC
1	Dodecanoic acid (Lauric acid)	$CH_3(CH_2)_{10}COOH$	C_{12}	5.45
2	Tetradecanoic acid (Myristic acid)	$CH_3(CH_2)_{12}COOH$	C_{14}	1.51
3	Hexadecanoic acid (Palmitic acid)	$CH_3(CH_2)_{14}COOH$	C_{16}	50.12
4	Octadecanoic acid (Stearic acid)	$CH_3(CH_2)_{16}COOH$	C_{18}	5.20
5	12-Octadecenoic acid (Oleic acid)	$C_{18}H_{32}O_2$	$C_{18:1}$	29.50
6	Linoleic acid	$C_{18}H_{32}O_2$	$C_{18:2}$	6.90

Table 8 Estimation of chloride content and foamability in soap bar with different concentration of nano ZnO-SPA.

Parameters	Soap without nano ZnO-SPA	0.5 mg/g	1.5 mg/g	2.5 mg/g
Foam Improvement %	0	7.55	16.98	28.3
Chloride content	0.5	0.57	0.71	0.85

3.3.1. Determination of chloride content

The chloride content as NaCl was evaluated by using wet analysis method there is significant change observed in the chloride content 0.7%, 1.4% and 2.1% after addition of nano ZnO-SPA 5 mg/mL, 10 mg/mL and 15 mg/mL of liquid cleansing product Fig. 8(A). The possible reason to increase of chloride content because of sodium chloride liberated as by product during the synthesis of nano ZnO-SPA. This additional electrolyte content in product play an important role in influencing the rheological properties of final product.

3.3.2. Determination of effect on rheological properties of liquid cleansing product

The rheological properties of liquid cleansing products were evaluated by Brookfield Rheometer DVT-3. The different concentrations of nano ZnO-SPA were added into the liquid cleansing product resulting into the change in rheology of liquid cleansing product. 2.17%, 4.16%, 7.69% increase in rheology (viscosity) observed after addition of 5 mg/mL, 10 mg/mL and 15 mg/mL of nano ZnO-SPA of liquid cleansing product shows in Fig. 8(B). Nano ZnO-SPA contain anionic surfactant (SLES-2EO) and the sodium chloride liberated as by product, most commonly electrolyte used in the liquid cleansing product to modify the rheology. The nano ZnO-SPA composition influence shape of anionic surfactant micelles and convert them into rod shape micellar arrangement in the presence of defined level of electrolyte and entanglement of these structure results in the increase of viscosity of liquid cleansing product.

3.4. Antibacterial properties of nano ZnO-SPA

Antibacterial properties of nano ZnO-SPA, surfactant polyol assembly (SPA) and AR Grade ZnO were investigated by ZOI through disk diffusion method also called as Kirby Bauer method (Fig. 9A and B).

Sample weight of 50 mg each was used for the ZOI study against both Gram-positive *(S. aureus)* and Gram-negative *(E. coli)* bacteria. The ZOI of SPA and AR Grade ZnO was found to be nil. However, nano ZnO-SPA have shown the average ZOI 13.5 mm, standard error 0.6, having *p-value* < 0.01 there is significant difference found in the ZOI study of nano ZnO-SPA versus AR Grade ZnO (Table 9). The higher antibacterial efficacy of nano ZnO is due to multiple reasons like higher active surface area available for the contact with microbes per unit mass. Slight lower activity against Gram-positive microbes could be due to their thicker layer of peptidoglycan in cell wall causing higher resistance to ZnO nanoparticles actions.

3.5. Antibacterial properties and application of nano ZnO-SPA infusion in sodium salt of long chain fatty acid

Photostability of soap matrix was studied into the direct sunlight comprising high energy UV rays which usually have detrimental impact on soap product stability and properties. Antibacterial properties of soap matrix infused with nano ZnO-SPA and without were investigated by standard log reduction method EN 1276:2019.

3.5.1. Photostability study of soap matrix having nano ZnO-SPA

Different concentrations of nano ZnO-SPA were used in soap bar (0.5 mg/g, 1.5 mg/g, 2.5 mg/g). Photostability study and color ordinate (L, a, b) measurement was carried out using Xrite Ci4200 reflectance spectrophotometer. Soap without nano ZnO shows reduction in the whiteness up to 17.85% leading towards yellow, red appearance of soap bar in comparison to initial whiteness when exposed to sunlight. However, soap bar infused with 0.5 mg nano ZnO-SPA per g of soap matrix shows a reduction in whiteness up to 15.69%, 1.5 mg nano ZnO-SPA per g of soap matrix shows a reduction in whiteness 11.81% and 2.5 mg nano ZnO-SPA per g of soap exhibits reduction whiteness only up to 7.9% which is significantly better than the soap without nano ZnO-SPA infusion

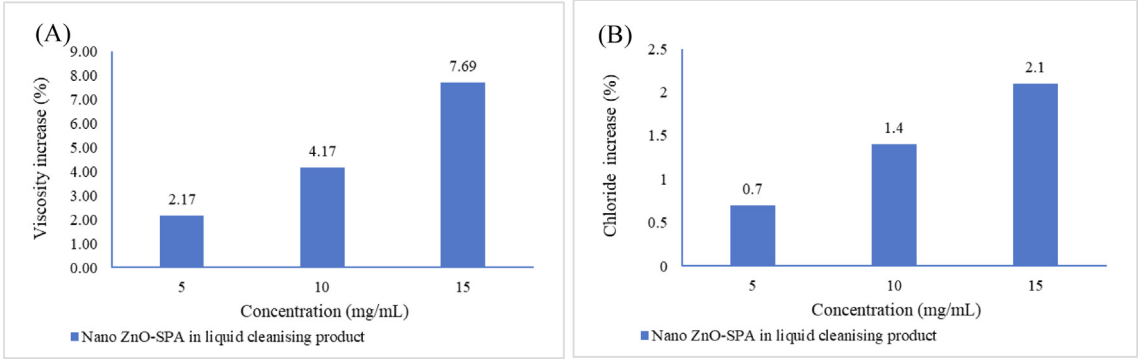

Fig. 8 (**A**) Effect of nano ZnO-SPA on chloride content of liquid cleansing product. (**B**) Effect of nano ZnO-SPA on rheological properties of liquid cleansing product.

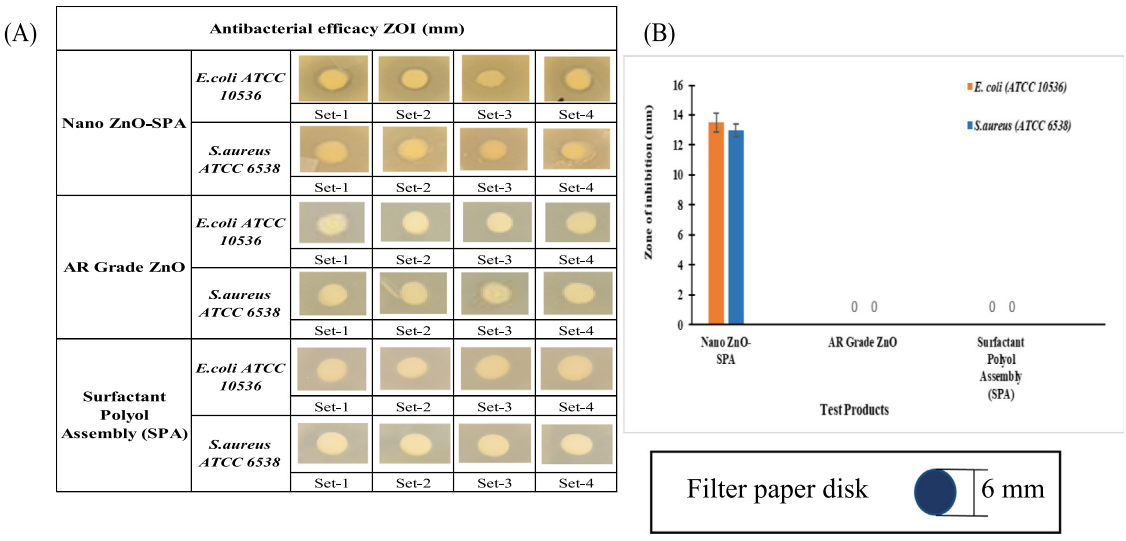

Fig. 9 (A) Pictorial and (B) Graphical representation of antibacterial activity (ZOI) of nano ZnO-SPA, AR Grade ZnO and SPA against *S. aureus* & *E. coli*.

Table 9 Antibacterial activity (ZOI in mm) of nano ZnO-SPA & AR Grade ZnO against *E. coli* and *S. aureus*.

Zone of inhibition (mm)							
Sr. no.	Name of product	*E. coli*			*S. aureus*		
		Average	Std. Deviation	Std. error	Average	Std. Deviation	Std. error
1	Nano ZnO-SPA	13.5	1.291	0.645	13	0.8165	0.4082
2	AR Grade ZnO	0	0	0	0	0	0
3	Surfactant Polyol Assembly (SPA)	0	0	0	0	0	0

(Fig. 10C). This study evidently shows that the nano ZnO-SPA even at lower concentrations significantly protects the products from direct sunlight and heat energy by acting in multiple manner like by scattering the light, absorbing the high energy UV-radiations of the sunlight which contributes towards free radicals, blocking the unsaturated site and possibly by scavenging the free radicals and eventually enhancing the photostability of soap bar. The mechanistic representation shown in Fig. 10(A and B).

3.5.2. EN 1276:2019 test (Soap Matrix)

The antibacterial efficacy of soap matrix infused without and with nano ZnO-SPA have been investigated as per EN-1276:2019 protocol. Results revealed the high potency of soap matrix with nano ZnO-SPA against both Gram-positive and Gram-negative bacteria. Soap infused with nano ZnO displayed 4.0 log reduction against Gram-positive and Gram-negative bacteria within 1 min contact time which is equivalent to killing of 99.99% of microbes. Whereas base soap without infusion of ZnO have shown nil reduction, in-fact displayed too numerous to count (TNTC) microbes. The values of bacterial log reduction obtained from test are presented (Table 10).

High antibacterial efficacy of soap infused with nano ZnO-SPA mainly due to active surface of ZnO disrupting the microbial cell wall, also presence of soap as a surfactant contributes in reducing the interfacial tension between ZnO and lipid bilayers of microbial cell wall.

3.6. Antibacterial properties and application of liquid cleansing product

Antibacterial properties of liquid cleansing products investigated by disk diffusion method (ZOI) using different concentration of nano ZnO-SPA (Fig. 11A and B). The antibacterial efficacy evaluation of liquid cleansing product infused with different concentration of nano ZnO-SPA was carried out using diffusion method to study ZOI. Four concentrations were studied for antibacterial efficacy, base liquid cleansing product does not show zone of inhibition action, nano ZnO-SPA 5 mg/mL of liquid cleansing product show the ZOI average diameter 6.87 mm, standard error 0.125, nano ZnO-SPA 10 mg/mL of liquid cleansing product shows the 9.75 mm ZOI and standard error 0.164, nano ZnO-SPA 15 mg/mL of liquid cleansing product exhibits the 11.75 mm ZOI with standard error 0.313 (Table 11). There are number of factors that can affect the ZOI in the study, such as material diffusion rate through agar, solubility, agar medium thickness variation, and concentration of impregnated material into the disk. Therefore, multiple set are recommended to have the statistical analysis and account for standard error and reflect the realistic potency of material.

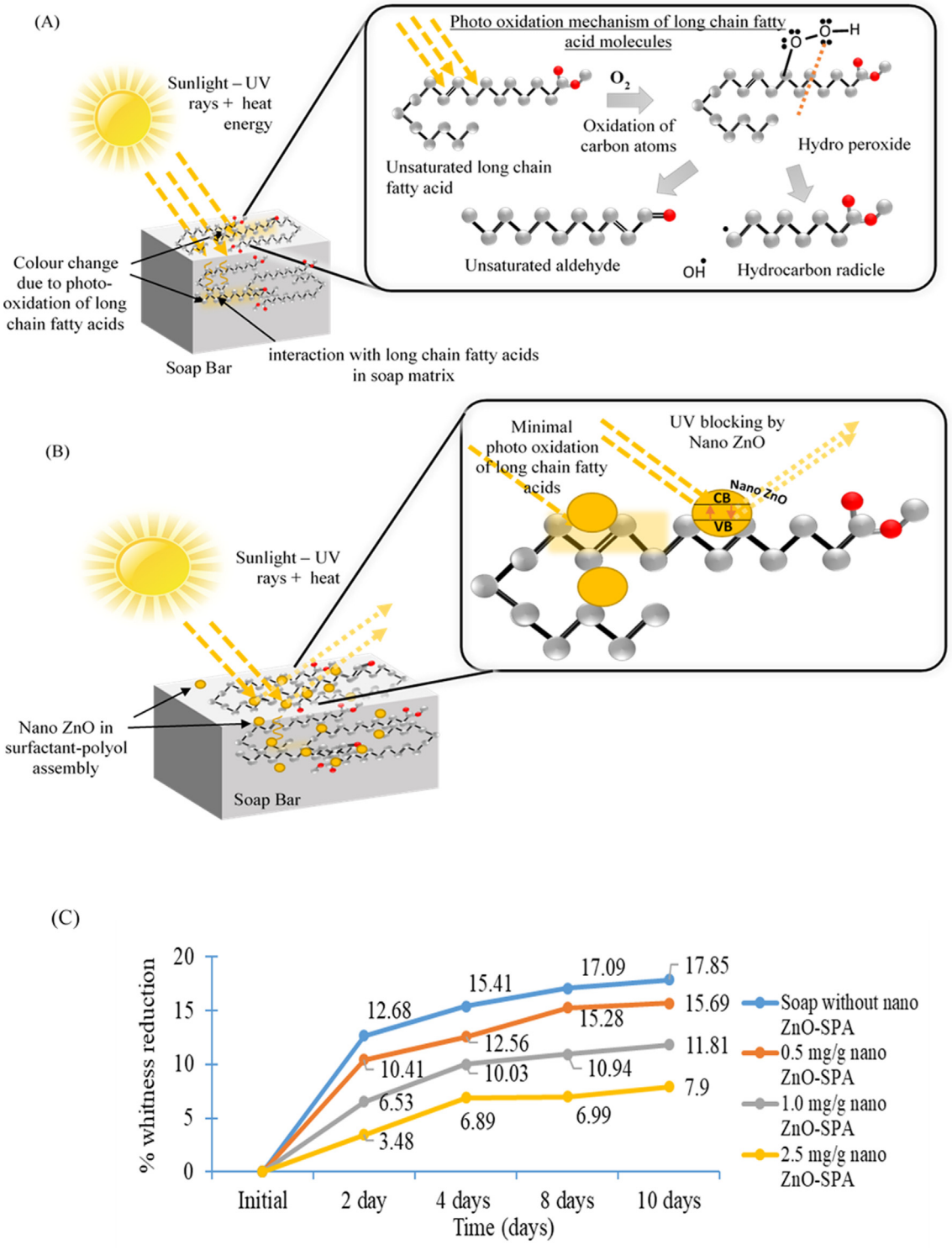

Fig. 10 (A) Mechanism of UV light exposure on the soap and shows the color change and free radical generation in fatty acid. (B) Systematic presentation of nano ZnO blocking phenomenon of UV rays to reduce the rate of color degradation. (C) Photostability study of soap matrix in direct sunlight for 10 days with different concentration of nano ZnO synthesized in SPA.

As per the above results it can be clearly stated that liquid cleansing product infused with nano ZnO-SPA shows the high antibacterial efficacy against both Gram-positive and Gram-negative pathogens. High antibacterial potency of nano ZnO-SPA could be due to multiple reasons like high active surface, defects, and surface charges. These particles possibly acting in multiple ways to inhibit and kill the microbes as explained in detail in below sections.

Table 10 Antibacterial efficacy (EN 1276:2019) of sodium salt of long chain fatty acid infused with nano ZnO-SPA and without.

Quantity of nano ZnO SPA/Soap	Test Parameter	Initial suspension	Test Suspension	Test suspension	Final count log	Bacterial effect on log reduction
		cfu/mL	log10	cfu/mL		
Soap Base	*E. coli*	3.3×10^7	7.52	1.225×10^3	TNTC	TNTC
	S. aureus	1.25×10^7	7.10	1.225×10^3	TNTC	TNTC
2.5 mg/g	*E. coli*	3.3×10^7	7.52	1.225×10^3	3.09	4.43
	S. aureus	1.25×10^7	7.10	1.225×10^3	3.09	4.01

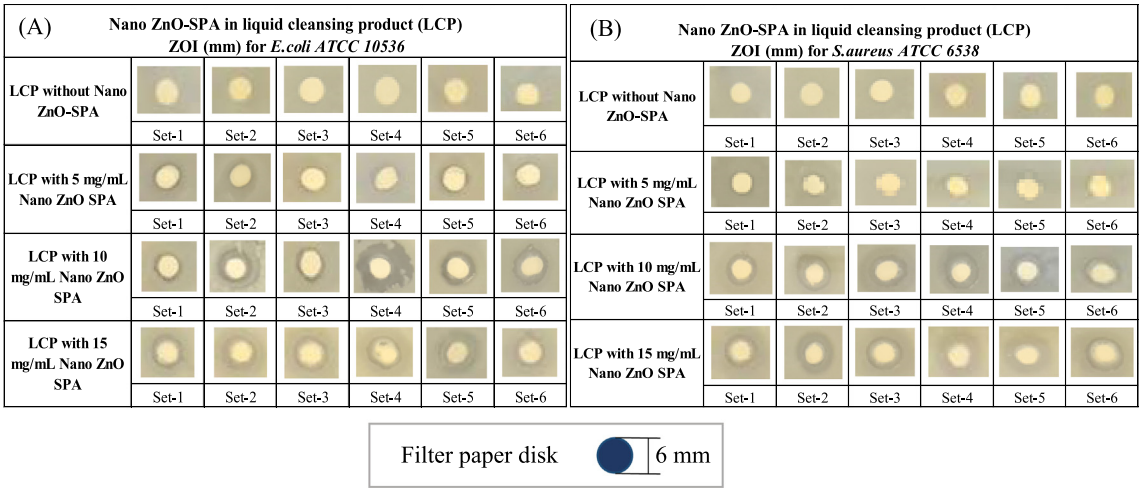

Fig. 11 Antibacterial efficacy (ZOI) (A) liquid cleansing product with and without nano ZnO-SPA against *E. coli* (B) liquid cleansing product with and without nano ZnO-SPA against S. *aureus*.

3.7. Possible mechanisms of antibacterial efficacy

High antibacterial efficacy of synthesized nano ZnO could be due to combination of multiple factors like availability of high surface area, porosity, surface defects, charges, their dissolution tendency, and release of Zn^{2+} and acting through different routes to kill and inhibit the microbes. Eccentric mechanisms of action which have been reported in the literatures such as: direct contact of nano ZnO molecule with the cell wall and subsequently destructing the integrity of bacterial cell (Brayner et al., 2006), interaction of Zn^{2+} ions for antibacterial activity (Cao et al., 2020), and generation of reactive oxygen species (ROS) (Fig. 12). However, the antibacterial mechanism may change according to the dissolved zinc and may change due to nano ZnO physiochemical properties (Lipovsky et al., 2011).

3.7.1. Generation of reactive oxygen species (ROS)

When the radiation of either matching or higher energy than bandgap is absorbed by ZnO, it triggers the generation of holes and electron excitement. The electron interacts with water (H_2O) to generate $^{\cdot}OH$ and H^+ as well as, O_2 molecules (suspended into mixture of nano ZnO and bacteria) to give super oxide anion. The super-oxide anion ($^{\cdot}O^{-2}$) reacts with the H^+

Table 11 Antibacterial efficacy (*ZOI* in mm) of liquid cleansing product infused with nano ZnO-SPA against *E. coli* and *S. aureus*.

Zone of inhibition (mm)						
Test product	*E. coli*			*S.aureus*		
	Average	Std. Deviation	Std. error	Average	Std. Deviation	Std. error
LCP without nano ZnO-SPA	0.000	0.000	0.000	0.000	0.000	0.000
LCP with 5 mg/mL nano ZnO-SPA	6.875	0.354	0.125	5.875	0.354	0.125
LCP with 10 mg/mL nano ZnO-SPA	9.750	0.463	0.164	9.625	0.518	0.183
LCP with 15 mg/mL nano ZnO-SPA	11.750	0.886	0.313	11.875	0.991	0.350

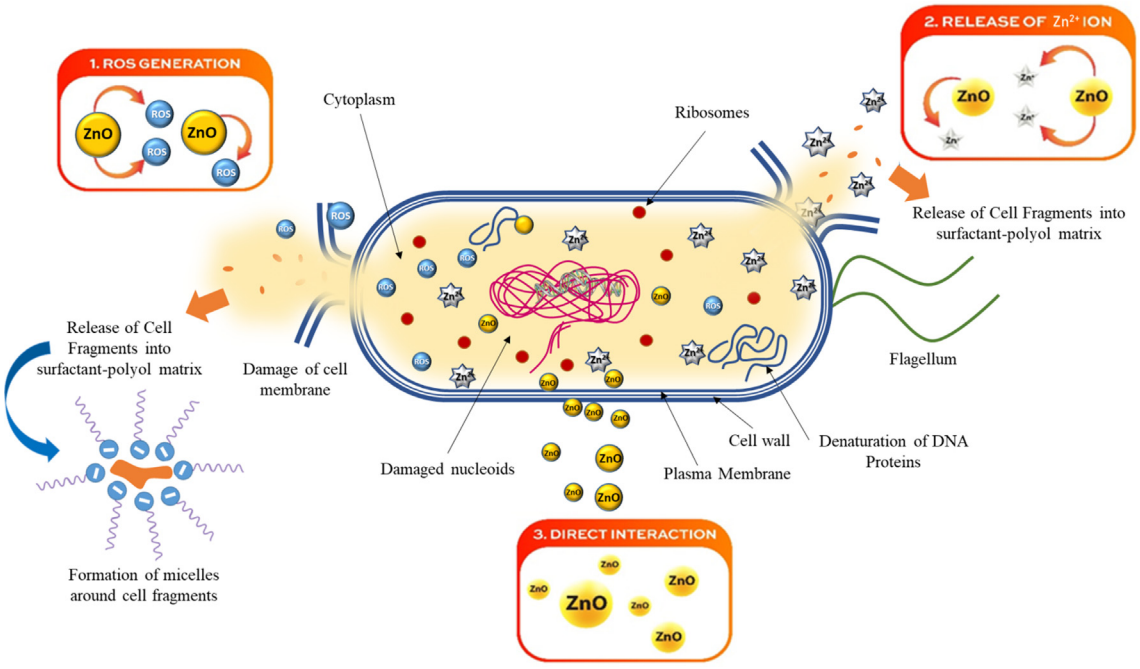

Fig. 12 Possible different mechanism of antibacterial action of nano ZnO-SPA, including: 1. ROS generation with release of cells fragment into SPA, 2. Release of Zn^{2+} ions, 3. Direct interaction of nano ZnO to cell wall.

to make up $\cdot HO_2$. Subsequently, HO_2 interfering with electrons to generates hydrogen peroxide ($\cdot HO_2$); which reacts with H^+ ions giving hydrogen peroxide (H_2O_2) molecules. The generation H_2O_2 mainly depends on the surface of nano ZnO to yield added active molecules. These ROS generated then disrupt the cell wall and damage the bacteria. The generation of ROS can be expressed by chemical equations as follows:

$$h\nu + ZnO \rightarrow e^- + h^+ \quad (9)$$

$$H_2O + h^+ \rightarrow \cdot OH + H^+(\quad 10)$$

$$e^- + O_2 \rightarrow \cdot O^-_2 \quad (11)$$

$$O_2 + H^+ \rightarrow \cdot HO_2 \quad (12)$$

$$HO_2 + H^+ + e^- \rightarrow H_2O_2 \quad (13)$$

3.7.2. Release of zinc ions (Zn^{2+})

Release of zinc ion is a vital antibacterial mechanism for nano ZnO which releases the zinc ions in medium of nano ZnO and bacterial cells. The Zn^{2+} shows the significant effect in disruption of enzyme, metabolism of amino acid, and inhibition of active transport (Song et al., 2010; Aydin Sevinç and Hanley, 2010). The antibacterial effect of nano ZnO limits due to insolubility and distribution of zinc ion into the medium. The medium component is responsible for dissolving zinc species and the physicochemical properties of nano ZnO. The Zn^{2+} release into medium is influenced by various physical, and chemical factors like size of nano ZnO, porosity, morphology, concentration, radiation, contact time, pH of medium and additional elements.

3.7.3. Direct interaction of nano ZnO to cell wall

Nano ZnO plays an important role on the antibacterial mechanism due to strong surface defects phenomenon and their surface charges. The nano ZnO have numerous edges on their surface due to which the surface site has been potentially active. The direct electrostatic interaction with cell wall severely influences cell wall of the bacteria. The damage of cell membrane by edges and corners, results from nano ZnO abrasive surface (Padmavathy and Vijayaraghavan, 2008). Various applications of nano ZnO can be accomplished by regulating the impurity, defects, morphologies, and their associated carrier charge (Schmidt-Mende and MacManus-Driscoll, 2007).

4. Conclusion

This presented study may be the first detailed research report on fabrication of nano ZnO in a unique surfactant polyol combination and established its applications through health and hygiene products. The synthesis causes in-situ generation of electrolyte influencing packing parameters of assembly and controlling the crystallite size in nano regime. This study further demonstrated antibacterial efficacies, and established performance advancement of health and hygiene products by infusing highly functional nano ZnO into sodium salts of long chain fatty acids (soap) and into liquid cleansing product. Employed advanced characterization techniques (UV–vis, FT-IR, SEM, EDAX, and XRD) confirmed the formation of ZnO and their crystallite size to be in nano regime (20–30 nm), band gap energy (3.66 eV) and high specific surface area (52.99 m^2/g). Further, the high antibacterial activity of nano ZnO-SPA materials were established using agar disk diffusion method and capturing the ZOI against Gram-positive (*S. aureus*) and Gram-negative organisms (*E. coli*). Application of the nano ZnO-SPA into sodium salt of long chain fatty acids matrix and liquid cleansing products confirmed significant antibacterial efficacies against disease causing germs. Multifunctional nano ZnO-SPA in soap matrix

act as an inorganic physical UV ray blocker reducing the rate of degradation of unsaturated fatty acids resulting into significant enhancement of photostability of soap and protect the whiteness of soap bar. Also, acting as a potent antibacterial agent through products when in use, demonstrated by ZOI and EN 1276:2019 methodologies up to 4.43 log reduction equivalent to 99.99% germ kill exhibited. Therefore, nano ZnO-SPA can be a next-generation antibacterial agent to kill a variety of disease-causing germs, can act as a theragnostic agent and is a suitable potent material for multidisciplinary industrial applications.

Acknowledgements

Authors are highly thankful to IFFCO group, UAE, especially Mr. Isa Allana-Managing director (MD), Mr. Serhad C. Kelemci-Chief executive officer (CEO), Mr. Sunil Singh-Technical director and NIT-Warangal's directors for their encouragement and continuous support for this study.

Declaration of Competing Interest

The authors hereby declare that there is no conflict of interest, neither in funding nor in interpreting the technical data and publishing the results.

References

Abendrot, M., Kalinowska-Lis, U., 2018. Zinc-containing compounds for personal care applications. Int. J. Cosmet. Sci. 40, 319–327. https://doi.org/10.1111/ics.12463.

Aydin Sevinç, B., Hanley, L., 2010. Antibacterial activity of dental composites containing zinc oxide nanoparticles. J. Biomed. Mater. Res. Part B: Appl. Biomater. 9999B, NA-NA. https://doi.org/10.1002/jbm.b.31620.

Azizi-Lalabadi, M., Ehsani, A., Divband, B., Alizadeh-Sani, M., 2019. Antimicrobial activity of Titanium dioxide and Zinc oxide nanoparticles supported in 4A zeolite and evaluation the morphological characteristic. Sci. Rep. 9. https://doi.org/10.1038/s41598-019-54025-0.

Bahadur, H., Srivastava, A., Sharma, R., Chandra, S., 2007. Morphologies of Sol-Gel Derived Thin Films of ZnO Using Different Precursor Materials and their Nanostructures. Nanoscale Res. Lett. 2. https://doi.org/10.1007/s11671-007-9089-x.

Beasley, D.G., Meyer, T.A., 2010. Characterization of the UVA Protection Provided by Avobenzone, Zinc Oxide, and Titanium Dioxide in Broad-Spectrum Sunscreen Products. Am. J. Clin. Dermatol. 11, 413–421. https://doi.org/10.2165/11537050-000000000-00000.

Boz, I., Kaluza, S., Boroğlu, M.S., Muhler, M., 2012. Synthesis of high surface area ZnO powder by continuous precipitation. Mater. Res. Bull. 47, 1185–1190. https://doi.org/10.1016/j.materresbull.2012.02.005.

Brayner, R., Ferrari-Iliou, R., Brivois, N., Djediat, S., Benedetti, M.F., Fiévet, F., 2006. Toxicological Impact Studies Based on Escherichia coli Bacteria in Ultrafine ZnO Nanoparticles Colloidal Medium. Nano Lett. 6, 866–870. https://doi.org/10.1021/nl052326h.

Cai, B., Zhao, X., Pei, T., Toninelli, E., Tang, Q., Tong, Y., Liu, Y., 2014. Conductive SnO2: Sb nanobelts as electrodes for detection of NO2 in ppb level with ultrahigh sensitivity. Appl. Phys. Lett. 104, 073112. https://doi.org/10.1063/1.4866275.

Cao, D., Shu, X., Zhu, D., Liang, S., Hasan, M., Gong, S., 2020. Lipid-coated ZnO nanoparticles synthesis, characterization and cytotoxicity studies in cancer cell. Nano Convergence 7. https://doi.org/10.1186/s40580-020-00224-9.

Cole, C., 2016. Sunscreen Formulation: Optimizing Efficacy of UVB and UVA Protection. Principles Practice Photoprotect. 275–287. https://doi.org/10.1007/978-3-319-29382-0_15.

Cunliffe, S., Martin, P., Baker, M., Mihailova, O., Martin, P., 2020. Near infrared absorption spectroscopy for the quantification of unsulfated alcohol in sodium lauryl ether sulfate. J. Near Infrared Spectrosc. 29, 11–23. https://doi.org/10.1177/0967033520963825.

Debanath, M.K., Karmakar, S., 2013. Study of blueshift of optical band gap in zinc oxide (ZnO) nanoparticles prepared by low-temperature wet chemical method. Mater. Lett. 111, 116–119. https://doi.org/10.1016/j.matlet.2013.08.069.

Gnanamozhi, P., Rajivgandhi, G., Alharbi, N.S., Kadaikunnan, S., Khaled, J.M., Almanaa, T.N., Pandiyan, V., Li, W.-J., 2020. Enhanced antibacterial and photocatalytic degradation of reactive red 120 using lead substituted ZnO nanoparticles prepared by ultrasonic-assisted co-precipitation method. Ceram. Int. 46, 19593–19599. https://doi.org/10.1016/j.ceramint.2020.05.020.

Goktas, A., Aslan, F., Yeşilata, B., Boz, İ., 2018. Physical properties of solution processable n-type Fe and Al co-doped ZnO nanostructured thin films: Role of Al doping levels and annealing. Mater. Sci. Semicond. Process. 75, 221–233. https://doi.org/10.1016/j.mssp.2017.11.033.

Goktas, S., Goktas, A., 2021. A comparative study on recent progress in efficient ZnO based nanocomposite and heterojunction photocatalysts: A review. J. Alloy. Compd. 863, 158734. https://doi.org/10.1016/j.jallcom.2021.158734.

Gomathi, M., Rajkumar, P.V., Prakasam, A., 2018. Study of dislocation density (defects such as Ag vacancies and interstitials) of silver nanoparticles, green-synthesized using Barleria cristata leaf extract and the impact of defects on the antibacterial activity. Results Phys. 10, 858–864. https://doi.org/10.1016/j.rinp.2018.08.011.

Halden, R.U., 2014. On the Need and Speed of Regulating Triclosan and Triclocarban in the United States. Environ. Sci. Technol. 48, 3603–3611. https://doi.org/10.1021/es500495p.

Hall, N., 2016. Implications of Soap Structure for Formulation and User Properties. Soap Manuf. Technol. 1–33. https://doi.org/10.1016/b978-1-63067-065-8.50001-3.

Hammoudeh, A.Y., Obeidat, S.M., Abboushi, E.K., Mahmoud, A.M., 2020. FT-IR Spectroscopy for the Detection of Diethylene Glycol (DEG) Contaminant in Glycerin-Based Pharmaceutical Products and Food Supplements. Acta Chim. Slov. 67, 530–536. https://doi.org/10.17344/acsi.2019.5553.

Haranath, D., Bhalla, N., Chander, H., Rashmi, Kar, M., Kishore, R., 2004. Controlled growth of ZnS: Mn nanophosphor in porous silica matrix. J. Appl. Phys. 96, 6700–6705. https://doi.org/10.1063/1.1806552.

Hasan, M., Altaf, M., Zafar, A., Hassan, S.G., Ali, Z., Mustafa, G., Munawar, T., Saif, M.S., Tariq, T., Iqbal, F., Khan, M.W., Mahmood, A., Mahmood, N., Shu, X., 2021. Bioinspired synthesis of zinc oxide nano-flowers: A surface enhanced antibacterial and harvesting efficiency. Mater. Sci. Eng., C 119, 111280. https://doi.org/10.1016/j.msec.2020.111280.

Hasnidawani, J.N., Azlina, H.N., Norita, H., Bonnia, N.N., Ratim, S., Ali, E.S., 2016. Synthesis of ZnO Nanostructures Using Sol-Gel Method. Procedia Chem. 19, 211–216. https://doi.org/10.1016/j.proche.2016.03.095.

Hattiangdi, G.S., 1949. Characterization of some commercial soaps by X-ray diffraction. National Bureau of Standards.

Huang, M.H., 2001. Room-Temperature Ultraviolet Nanowire Nanolasers. Science 292, 1897–1899. https://doi.org/10.1126/science.1060367.

Imran, M., Haider, S., Ahmad, K., Mahmood, A., Al-masry, W.A., 2017. Fabrication and characterization of zinc oxide nanofibers for renewable energy applications. Arabian J. Chem. 10, S1067–S1072. https://doi.org/10.1016/j.arabjc.2013.01.013.

IS 13498, 1997. Bathing bars [CHD 25: Soaps and other Surface-Active Agents].

Isa, E.D.M., Shameli, K., Jusoh, N.W.C., Hazan, R., 2020. Rapid photodecolorization of methyl orange and rhodamine B using zinc oxide nanoparticles mediated by pullulan at different calcination conditions. J. Nanostruct. Chem. 11, 187–202. https://doi.org/10.1007/s40097-020-00358-6.

Jandacek, R.J., Broering, W.B., 1989. X-Ray diffraction study of sodium soaps of monounsaturated and polyunsaturated fatty acids. Lipids 24, 1008–1013. https://doi.org/10.1007/bf02544070.

Jin, S.-E., Jin, H.-E., 2021. Antimicrobial Activity of Zinc Oxide Nano/Microparticles and Their Combinations against Pathogenic Microorganisms for Biomedical Applications: From Physicochemical Characteristics to Pharmacological Aspects. Nanomaterials 11, 263. https://doi.org/10.3390/nano11020263.

Khezami, L., Ismail, M., Taha, K., Modwi, A., 2018. ZnO nanoparticles: Surface and X-ray profile analysis ZnO NANOPARTICLES: SURFACE AND X-RAY PROFILE ANALYSIS. J. Ovonic Res. 14, 381–393.

Khullar, V., Soni, S., Tyagi, H., 2016. Nanoparticle-Laden Flow for Solar Absorption. Handbook Multiphase Flow Sci. Technol. 1–30. https://doi.org/10.1007/978-981-4585-86-6_19-1.

Kong, X.Y., Wang, Z.L., 2003. Spontaneous Polarization-Induced Nanohelixes, Nanosprings, and Nanorings of Piezoelectric Nanobelts. Nano Lett. 3, 1625–1631. https://doi.org/10.1021/nl034463p.

Kumar, S., Jeon, H.C., Kang, T.W., Seth, R., Panwar, S., Shinde, S. K., Waghmode, D.P., Saratale, R.G., Choubey, R.K., 2019. Variation in chemical bath pH and the corresponding precursor concentration for optimizing the optical, structural and morphological properties of ZnO thin films. J. Mater. Sci.: Mater. Electron. 30, 17747–17758. https://doi.org/10.1007/s10854-019-02125-y.

Kumar, S., Mudai, A., Roy, B., Basumatary, I.B., Mukherjee, A., Dutta, J., 2020. Biodegradable Hybrid Nanocomposite of Chitosan/Gelatin and Green Synthesized Zinc Oxide Nanoparticles for Food Packaging. Foods 9, 1143. https://doi.org/10.3390/foods9091143.

Kumar, S., Seth, R., Panwar, S., Goyal, K.K., Kumar, V., Choubey, R.K., 2021. Morphological and Optical Studies of ZnO-Silica Nanocomposite Thin Films Synthesized by Time Dependent CBD. J. Electron. Mater. 50, 3462–3470. https://doi.org/10.1007/s11664-021-08863-2.

Lei, Y., Qu, F., Wu, X., 2012. Assembling ZnO Nanorods into Microflowers through a Facile Solution Strategy: Morphology Control and Cathodoluminescence Properties. Nano-Micro Lett. 4, 45–51. https://doi.org/10.1007/bf03353691.

Lipovsky, A., Nitzan, Y., Gedanken, A., Lubart, R., 2011. Antifungal activity of ZnO nanoparticles—the role of ROS mediated cell injury. Nanotechnology 22, 105101. https://doi.org/10.1088/0957-4484/22/10/105101.

Lodén, M., Wessman, W., 2001. The influence of a cream containing 20% glycerin and its vehicle on skin barrier properties. Int. J. Cosmet. Sci. 23, 115–119. https://doi.org/10.1046/j.1467-2494.2001.00060.x.

Mishra, S., Supraja, P., Jaiswal, V.V., Sankar, P.R., Kumar, R.R., Prakash, K., Kumar, K.U., Haranath, D., 2021. Enhanced output of ZnO nanosheet-based piezoelectric nanogenerator with a novel device structure. Eng. Res. Express 3, 045022. https://doi.org/10.1088/2631-8695/ac34c3.

Nazir, A., Akbar, A., Baghdadi, H.B., ur Rehman, S., Al-Abbad, E., Fatima, M., Iqbal, M., Tamam, N., Alwadai, N., Abbas, M., 2021. Zinc oxide nanoparticles fabrication using Eriobotrya japonica leaves extract: Photocatalytic performance and antibacterial activity evaluation. Arabian J. Chem. 14, 103251. https://doi.org/10.1016/j.arabjc.2021.103251.

Oprea, O., Andronescu, E., Vasile, B., Voicu, G., Covaliu, C., 2011. Synthesis and characterization of ZnO nanopowder by non-basic route. Digest J. Nanomater. Biostruct. 6, 1393–1401.

Padmavathy, N., Vijayaraghavan, R., 2008. Enhanced bioactivity of ZnO nanoparticles—an antimicrobial study. Sci. Technol. Adv. Mater. 9, 035004. https://doi.org/10.1088/1468-6996/9/3/035004.

Peretz, S., Anghel, D., Stoian, C., n.d. Chitosan microparticulate systems prepared by polymer-surfactant interaction.

Rajamanickam, D., Shanthi, M., 2016. Photocatalytic degradation of an organic pollutant by zinc oxide – solar process. Arabian J. Chem. 9, S1858–S1868. https://doi.org/10.1016/j.arabjc.2012.05.006.

Rajapriya, M., Sharmili, S.A., Baskar, R., Balaji, R., Alharbi, N.S., Kadaikunnan, S., Khaled, J.M., Alanzi, K.F., Vaseeharan, B., 2019. Correction to: Synthesis and Characterization of Zinc Oxide Nanoparticles Using Cynara scolymus Leaves: Enhanced Hemolytic, Antimicrobial, Antiproliferative, and Photocatalytic Activity. J. Cluster Sci. 31. https://doi.org/10.1007/s10876-019-01734-1. 803–803.

Saleem, S., Jameel, M.H., Akhtar, N., Nazir, N., Ali, A., Zaman, A., Rehman, A., Butt, S., Sultana, F., Mushtaq, M., Zeng, J.H., Amami, M., Althubeiti, K., 2022. Modification in structural, optical, morphological, and electrical properties of zinc oxide (ZnO) nanoparticles (NPs) by metal (Ni, Co) dopants for electronic device applications. Arabian J. Chem. 15, 103518. https://doi.org/10.1016/j.arabjc.2021.103518.

Samavati, Z., Samavati, A., Ismail, A.F., Borhani, T.N., Velashjerdi, M., Eisaabadi, B.G., Rostami, A., Othman, M.H.D., Awang, A., 2021. Enhancement of organic solar cell efficiency by altering the zinc oxide photoanode nanostructure morphology. J. Nanostruct. Chem. https://doi.org/10.1007/s40097-021-00453-2.

Sánchez-Martín, S., Olaizola, S.M., Castaño, E., Urionabarrenetxea, E., Mandayo, G.G., Ayerdi, I., 2021. Study of deposition parameters and growth kinetics of ZnO deposited by aerosol assisted chemical vapor deposition. RSC Adv. 11, 18493–18499. https://doi.org/10.1039/d1ra03251h.

Schmidt-Mende, L., MacManus-Driscoll, J.L., 2007. ZnO – nanostructures, defects, and devices. Mater. Today 10, 40–48. https://doi.org/10.1016/s1369-7021(07)70078-0.

Shaban, M., Mohamed, F., Abdallah, S., 2018. Production and Characterization of Superhydrophobic and Antibacterial Coated Fabrics Utilizing ZnO Nanocatalyst. Sci. Rep. 8. https://doi.org/10.1038/s41598-018-22324-7.

Smijs, T., Pavel, 2011. Titanium dioxide and zinc oxide nanoparticles in sunscreens: focus on their safety and effectiveness. Nanotechnol. Sci. Appl. 95. https://doi.org/10.2147/nsa.s19419.

Song, W., Zhang, J., Guo, J., Zhang, J., Ding, F., Li, L., Sun, Z., 2010. Role of the dissolved zinc ion and reactive oxygen species in cytotoxicity of ZnO nanoparticles. Toxicol. Lett. 199, 389–397. https://doi.org/10.1016/j.toxlet.2010.10.003.

Vasile, O.-R., Andronescu, E., Ghitulica, C., Vasile, B.S., Oprea, O., Vasile, E., Trusca, R., 2012. Synthesis and characterization of nanostructured zinc oxide particles synthesized by the pyrosol method. J. Nanopart. Res. 14. https://doi.org/10.1007/s11051-012-1269-7.

Wirunchit, S., Gansa, P., Koetniyom, W., 2021. Synthesis of ZnO nanoparticles by Ball-milling process for biological applications. Mater. Today:. Proc. https://doi.org/10.1016/j.matpr.2021.03.559.

Yang, Y.H., Chen, X.Y., Feng, Y., Yang, G.W., 2007. Physical Mechanism of Blue-Shift of UV Luminescence of a Single Pencil-Like ZnO Nanowire. Nano Lett. 7 (12), 3879–3883. https://doi.org/10.1021/nl071849h.

Zhang, H., Liang, Z., Zhang, J., Wang, W., Zhang, H., Lu, Q., 2020. Zinc oxide nanoparticle synthesized from Euphorbia fischeriana root inhibits the cancer cell growth through modulation of apoptotic signaling pathways in lung cancer cells. Arabian J. Chem. 13, 6174–6183. https://doi.org/10.1016/j.arabjc.2020.05.020.